The Behavior of the Bulk − Skin Sea Surface Temperature Difference under Varying Wind Speed and Heat Flux

GARY A. WICK, WILLIAM J. EMERY, AND LAKSHMI H. KANTHA

Colorado Center for Astrodynamics Research, University of Colorado, Boulder, Colorado

PETER SCHLÜSSEL

Meteorologisches Institut, Universitaet Hamburg, Hamburg, Germany

(Manuscript received 2 August 1994, in final form 4 August 1995)

ABSTRACT

The observed and predicted response of the bulk − skin sea surface temperature difference (ΔT) to changes in the wind speed and net heat flux is analyzed. Observations of ΔT from the northern Atlantic and tropical Pacific Oceans demonstrate that the wind speed affects ΔT through the net heat flux and turbulent mixing. Increased winds typically increase the net heat flux, which increases the size of ΔT. At the same time, increased winds cause enhanced mixing, which decreases the size of ΔT. To predict the net change to ΔT, both effects must be properly modeled. The theoretical development of existing models for ΔT is traced and compared. All the models can be similarly derived from surface renewal theory with their differences resulting only from the corresponding definition of the dissipation rate. The differences are manifested in the predicted dependence of ΔT on the wind speed. The predicted ΔT values and wind speed dependencies are evaluated with the available ΔT observations to determine the most accurate approach. A new model for ΔT is developed to better reproduce the observed behavior of ΔT. The new model follows from surface renewal theory and includes timescales for both the shear-driven and free convection regimes. The model is shown to accurately reproduce both aspects of the observed effect of wind speed on ΔT and predict the value of ΔT to better than 0.1 K.

1. Introduction

The bulk − skin sea surface temperature difference (ΔT) refers to the temperature gradient that exists across the molecular boundary layer at the surface of the ocean. Viscous effects dominate in the molecular boundary layer and heat transfer occurs by molecular processes. The thickness of the molecular boundary layer is typically less than 1 mm (Grassl 1976). The ocean skin comprises the top few molecules of the molecular boundary layer. The ocean skin is generally a few tenths of a degree cooler than the water between the base of the molecular boundary layer and several meters below the surface due to the nature of the heat transfer at the ocean surface (McAlister and McLeish 1969; Hasse 1971; Grassl 1976; Robinson et al. 1984; Coppin et al. 1991). The existence of this temperature difference has an important effect on air–sea exchange processes and the measurement of sea surface temperature (SST) from satellites.

Many studies have investigated the parameters that govern the behavior of ΔT (Ewing and McAlister 1960; Saunders 1967; McAlister and McLeish 1969; Hasse 1971; Paulson and Parker 1972; Grassl 1976; Katsaros 1977; Liu et al. 1979; Katsaros 1980; Paulson and Simpson 1981; Schlüssel et al. 1990; Coppin et al. 1991; Soloviev and Schlüssel 1994). The precise effect of wind speed on ΔT is still unclear, however. The various theoretical predictions differ on the dependence of ΔT on wind speed. Some models (e.g., Saunders 1967) predict that ΔT is inversely proportional to the friction velocity while others (e.g., Brutsaert 1975a) predict a more complicated dependence where the wind speed appears in the model via the roughness Reynolds number. Similarly, different in situ datasets appear to suggest different effects of wind speed on ΔT. Fairall et al. (1996) noted that in skin temperature measurements taken by Schlüssel et al. (1990) the largest ΔT values occurred at high wind speeds, while in measurements taken by Coppin et al. (1991) the largest ΔT values occurred at low wind speeds.

The purpose of this paper is to investigate the wind speed dependence of ΔT. Both in situ data and theoretical predictions are examined to clarify the effect of wind speed on ΔT. Since ΔT also depends on the net heat flux and the net heat flux varies with the wind speed, the dependence of ΔT on the net heat flux is

Corresponding author address: Dr. Gary A. Wick, Applied Physics Laboratory, College of Ocean and Fishery Sciences, University of Washington, 1013 NE 40th Street, Seattle, WA 98105-6698.
E-mail: wick@apl.washington.edu

studied simultaneously. Two datasets containing measurements of ΔT are used to study the observed dependence of ΔT on wind speed under different climatological conditions. The development and predicted behavior of various theoretical models for ΔT are presented and compared. The modeled ΔT values are compared with the in situ observations to determine which theoretical approach most accurately predicts the dependence of ΔT on wind speed. Based on these results, a new model is derived for the prediction of ΔT.

2. In situ data

Two recent datasets contain accurate measurements of ΔT, wind speed, and the additional meteorological quantities required to compute the net heat flux using the bulk aerodynamic formulas. The first was collected aboard the German F/S *Meteor* in the northeast Atlantic Ocean in October and November of 1984. Measurements were collected between 21° and 50°N, 0° and 28°W. The conditions included in the dataset are representative of relatively dry midlatitude conditions. The second dataset was collected in March 1993 in the equatorial Pacific aboard the R/V *John V. Vickers* as part of the Central Equatorial Pacific Experiment (CEPEX). The section of the cruise used in this analysis extended between 2°N and 2°S from 165°E to 150°W. The corresponding conditions were representative of moist tropical conditions.

The measurements collected during both cruises consist of skin and bulk SST, downwelling solar and longwave radiation, wind speed, air temperature, and humidity. On the *Meteor,* the skin temperature was measured with a Barnes PRT-5 radiometer and the bulk temperature was measured with platinum resistance temperature devices (RTDs) at depths of 0.1, 2, 4, and 7 m beneath the surface. Further details on the *Meteor* measurements, their accuracy, and an analysis of the data were presented by Schlüssel et al. (1990). On the *Vickers,* the skin temperature was measured by the new Ophir Multi-Band Infrared Sea-Truth Calibrator (MISTRC) and the bulk temperature was measured at a depth of roughly 3 m with a precision thermistor. The downwelling solar and longwave radiation were measured with an Eppley pyranometer and pyrgeometer, respectively. The radiation sensors were gimbaled to eliminate effects of ship roll. The measurements were processed following Schlüssel et al. (1990) to provide an accuracy of about 10 W m^{-2}. The wind speed, air temperature, and humidity were measured with sensors operated by the ship. Documents provided by the crew of the *Vickers* list the accuracy of the bulk SST as 0.1 K, the air temperature as 0.3 K, and the relative humidity as 3%.

The Ophir MISTRC took measurements at wavelengths of 3.728, 4.025, 10.752, and 11.785 μm. In addition, the measurements at 3.728 and 4.025 μm were taken both with and without a vertical polarizer. The skin temperature measurements at each wavelength and polarization were independently calibrated in an identical manner using a well-mixed seawater reference following Schlüssel et al. (1990). The results showed discrepancies up to 0.1 K between the different measurements. The differences were similar during both day and night, implying that the differences were not caused by reflected solar radiation. The precise source of the differences is still being investigated, but the differences suggest that the seawater reference calibration system is not adequately correcting for effects due to the nonblackness of the sea surface. The net effect on this study is to add an additional uncertainty to the accuracy of the radiometric skin temperature measurements. Single wavelength measurements cannot show this problem, and thus the uncertainty is believed to apply to the *Meteor* measurements as well. The differences between the MISTRC measurements suggest a skin temperature uncertainty of 0.1 K. Standard error analysis for the computation of skin temperature from the reference system indicates errors of only 0.05 K. For this work, the accuracy of all skin temperature measurements was assumed to be 0.1 K.

TABLE 1. Average ΔT values (K) computed for wind speeds above and below 5 m s^{-1}.

Dataset	$u < 5$ m s^{-1}	$u > 5$ m s^{-1}
Meteor	0.27	0.34
CEPEX	0.23	0.20

The skin temperature measurements from the 4.025-μm polarized channel were used because they had the lowest noise level. The temperatures were increased by 0.07 K to force average agreement with the 10.752-μm measurements. The 10.752-μm average was selected for consistency with the PRT-5 radiometer used for the *Meteor* cruise.

Further analysis of the *Meteor* data since the paper by Schlüssel et al. (1990) indicated a possible problem with the accuracy of the bulk temperature measurements at 2-m depth. The 2-m temperature was consistently about 0.05 K cooler than both the 4-m and 7-m temperatures, even during periods of strong mixing when no offset is expected. When the measurements at 0.1 m were available, they agreed more closely with the 4-m measurements than the 2-m measurements. The ΔT values for the *Meteor* data were, therefore, calculated relative to the 4-m bulk temperature rather than the 2-m bulk temperature as in Schlüssel et al. (1990).

Hourly averages of ΔT and all meteorological measurements were calculated for both datasets. Measurements were only considered when all quantities required to calculate the net heat flux were available. Measurements where the wind speed was greater than 10 m s^{-1} or the skin temperature was greater than the

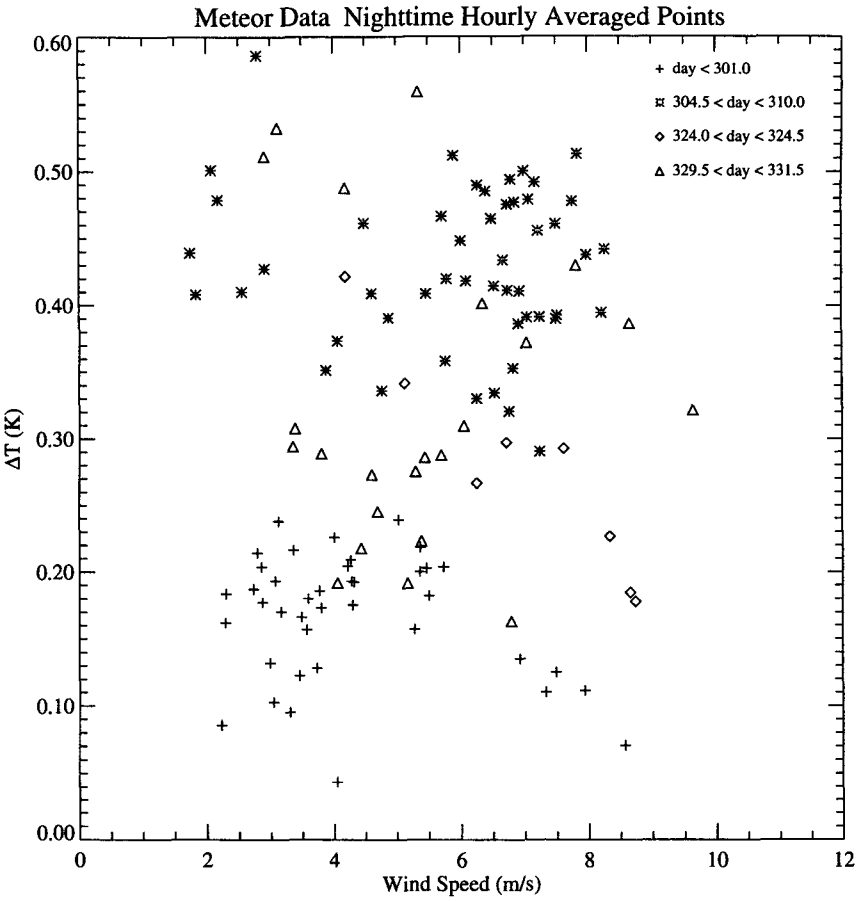

FIG. 1. Relationship between ΔT and wind speed for hourly averages of nighttime measurements from the F/S *Meteor*. The different symbols correspond to different segments of the cruise as indicated in the legend. Note that there is no apparent relationship between ΔT and wind speed during any of the cruise segments. The correlation coefficient for all of the points grouped together is 0.19.

bulk temperature at night were also eliminated. All analyses were limited to the nighttime to eliminate any possible effects of daytime warming of the near-surface layer in the ocean. The heat flux was computed from the averaged meteorological measurements using the bulk aerodynamic formulae following the approach of Clayson et al. (1996). Hourly averages were used to reduce the random errors associated with individual ΔT measurements and to improve the approximations involved in the use of the bulk aerodynamic formula.

Following Schlüssel et al. (1990) the average ΔT for wind speeds both above and below 5 m s^{-1} was calculated for each dataset. The results are shown in Table 1. As found by Schlüssel et al. (1990), the largest ΔT values in the *Meteor* dataset occur at the highest wind speeds. In contrast, though there is only a small change in the average ΔT values, the largest ΔT values in the CEPEX dataset occur at the lowest wind speeds. This is the same contrast noted by Fairall et al. (1996) between the Schlüssel et al. (1990) and Coppin et al. (1991) datasets.

To further investigate this difference and determine what the in situ data reveals about the relationship between wind speed and ΔT, the hourly averaged nighttime ΔT values were plotted against the corresponding hourly averages of the wind speed. The results from the *Meteor* are shown in Fig. 1, while the results from CEPEX are shown in Fig. 2. Though the average ΔT is greater at higher wind speeds for the *Meteor* data, there is no significant correlation between ΔT and wind speed. There are also large ΔT values at low wind speeds and low ΔT values at high wind speeds. Even when the *Meteor* data is broken into small segments with similar conditions, there is no significant correlation between ΔT and wind speed during those periods. Similarly, the CEPEX data shows only a small tendency for ΔT to decrease as the wind speed increases. The correlation coefficient is only -0.22. Plotting ΔT against the friction velocity, u_*, in place of the wind speed does not significantly change the appearance of the plots. Based on the degree of scatter in both data-

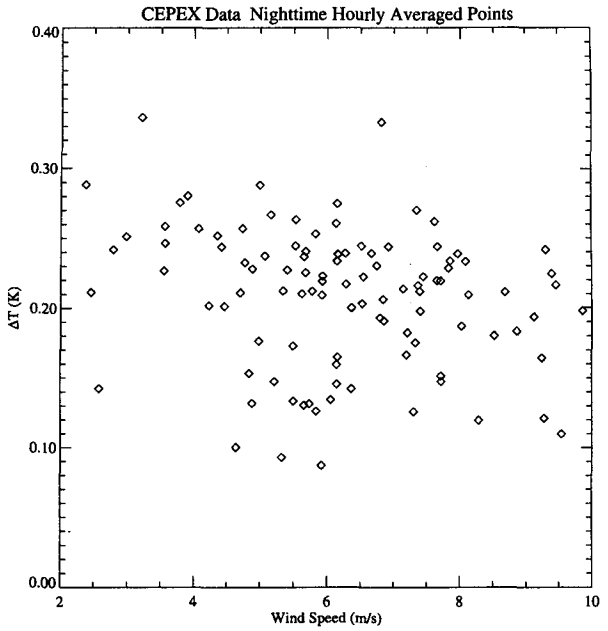

FIG. 2. Relationship between hourly averages of nighttime measurements of ΔT and wind speed from the CEPEX data. The correlation coefficient is only -0.22, indicating that no significant correlation between ΔT and wind speed was observed in the data.

sets, the datasets cannot be said to show significantly different behavior. It is impossible to conclude from these figures how ΔT responds to a change in wind speed. The effect of wind speed on ΔT cannot be determined while ignoring the effect of other parameters that influence ΔT.

To isolate the dependence of ΔT on wind speed while still accounting for variations in ΔT due to changes in the net heat flux, we used three-dimensional projections to plot ΔT as a simultaneous function of wind speed and net heat flux. The nighttime ΔT values from each dataset were binned by wind speed and heat flux values, and an average ΔT was computed for each bin. A ΔT value of 0 was assigned if there were no data available for the bin. Although 0 is a reasonable ΔT value, it was chosen for the no-data value to give the plots the best clarity. The heat flux is defined as positive from the ocean to the atmosphere, the normal orientation for nighttime conditions.

The results for the *Meteor* and CEPEX data are shown in Figs. 3a and 3b, respectively. When plotted in this manner, the datasets show similar overall trends. Both datasets show that ΔT increases with the net heat flux when the wind speed is held constant and that ΔT generally decreases with increasing wind speed if the net heat flux is held constant. The rate of change of ΔT with wind speed is greatest at the lowest wind speeds. The most significant difference between the datasets is in the rate of increase in ΔT with increasing net heat flux. The data from the *Meteor* suggest a much greater rate of increase.

The surfaces suggest a two-part dependence of ΔT on wind speed through turbulent mixing and the net heat flux. First, an increase in wind speed increases the turbulent mixing near the ocean surface that acts to decrease the temperature gradient across the molecular boundary layer. Second, increases in the wind speed also cause an increase in the net heat flux which increases the cooling at the surface and increases ΔT. If wind speed and heat flux were independent, it could be concluded that ΔT increases with heat flux and decreases with wind speed. Since the heat flux and wind speed are related, the precise state of the measurement must be known. If a decrease in wind speed leads only to a small change in the heat flux, ΔT will likely increase. If instead a decrease in wind speed leads to a significant drop in the heat flux such as when the latent heat flux dominates, ΔT will probably decrease.

The different appearance of Figs. 1 and 2 is caused by the different rates of increase of ΔT with net heat flux and the different relative effect of wind speed on the net heat flux. A scatterplot of the net heat flux versus wind speed for both datasets is shown in Fig. 4. Over the same approximate wind speed range, the net heat flux varies by 275 W m^{-2} in the *Meteor* data in comparison with only 200 W m^{-2} in the CEPEX data. A change in wind speed is typically accompanied by a larger change in net heat flux in the *Meteor* data. The response of ΔT to the change in net heat flux overwhelms the response to the change in wind speed especially for the observed sharp response of ΔT to the heat flux in the *Meteor* data. As a result, the correlation between ΔT and wind speed is reduced for the *Meteor* data as seen in Fig. 1. The effect of the varying response of net heat flux to changes in wind speed will be discussed further in section 4a.

3. Theoretical predictions

To accurately predict ΔT and properly account for its effects, theoretical ΔT models must be able to reproduce this observed behavior. The current models for ΔT all generally predict the observed two-part dependence of ΔT on wind speed, but differ on the precise functional dependence on wind speed. The derivations are similar, but slight differences have a significant effect on the predicted response to wind speed. It is necessary to compare the different predicted relationships and determine which is most accurate.

a. Current ΔT models

Several different theories have been developed to predict the functional dependence of ΔT on the net heat flux and wind speed (Saunders 1967; Hasse 1971; Paulson and Parker 1972; Brutsaert 1975a; Grassl

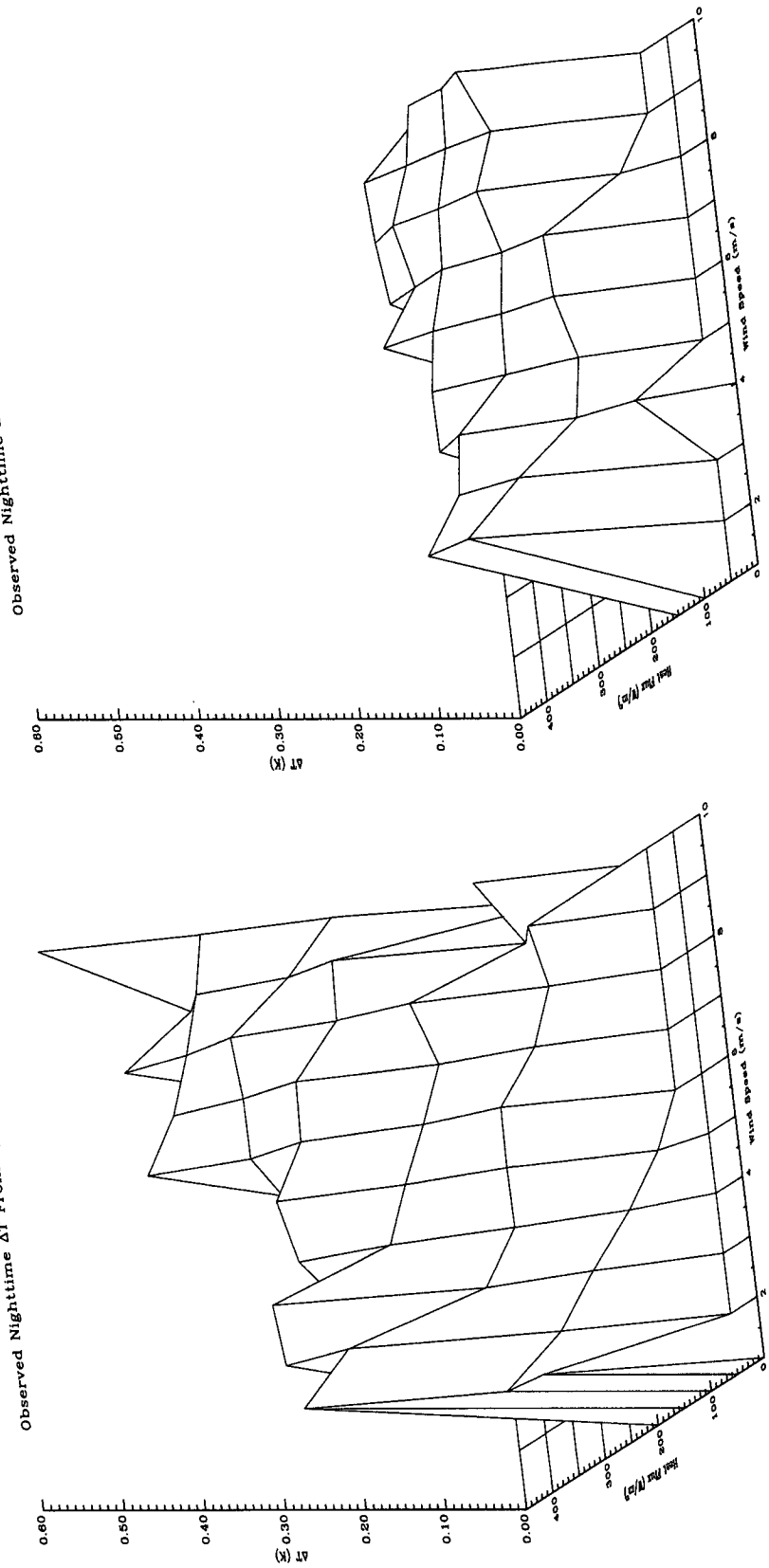

FIG. 3. Observed response of nighttime ΔT measurements to changes in net heat flux and wind speed in the (a) *Meteor* and (b) CEPEX datasets. Values of 0 indicate that no data was available for the corresponding bin. There is a tendency in both datasets for ΔT to increase with increasing net heat flux and decrease with increasing wind speed.

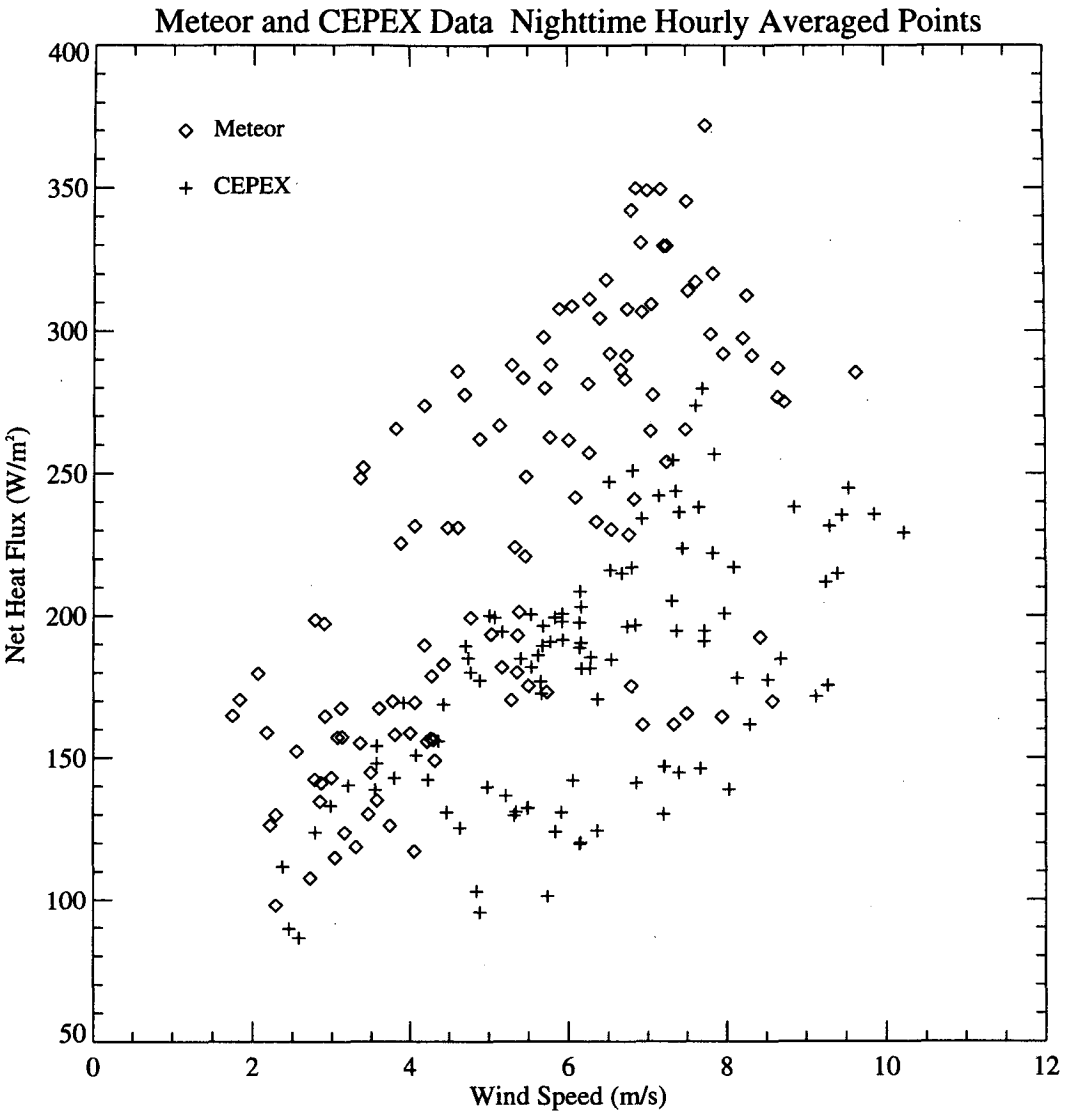

FIG. 4. Observed relationship between nighttime measurements of net heat flux and wind speed in the *Meteor* and CEPEX datasets. The correlation coefficient is 0.70 for the points from the *Meteor* and 0.61 for the CEPEX data. The net heat flux increases with increasing wind speed in both datasets, but for the same change in wind speed, the net heat flux increases by a greater amount in the *Meteor* data.

1976; Katsaros 1977; Liu et al. 1979; Paulson and Simpson 1981; Robinson et al. 1984; Wu 1985; Schlüssel et al. 1990; Coppin et al. 1991; Soloviev and Schlüssel 1994). The first model of ΔT was presented by Saunders (1967, hereafter referred to as Saunders). The Saunders model is based on the assumption that the heat transfer across the skin layer occurs by molecular conduction. For molecular conduction, the temperature gradient is given by

$$\Delta T = \frac{Q_N \delta}{k}, \tag{1}$$

where Q_N is the net heat flux, δ is the thickness of the skin layer, and k is the thermal conductivity of seawater. The difficulty in applying (1) is determining the thickness of the skin layer. From dimensional arguments, Saunders assumed that δ is given by

$$\delta \propto \frac{\nu}{u_*}, \tag{2}$$

where ν is the kinematic viscosity of water and u_* is the friction velocity of the water. The friction velocity is related to the wind speed by

$$u_* = \sqrt{\frac{\rho_a}{\rho_w} C_D u^2}, \quad (3)$$

where u is the wind speed, C_D is the drag coefficient, and ρ_a and ρ_w are the density of air and seawater, respectively. Inserting (2) into (1) gives the Saunders model for ΔT:

$$\Delta T = \lambda \frac{Q_N \nu}{u_* k}, \quad (4)$$

where λ is a constant of proportionality. Saunders did not have data to determine the value of λ but estimated it to be between 5 and 10.

Since then, many investigators have determined values for λ. Much of the work focused on whether λ is truly a constant. Paulson and Parker (1972), Paulson and Simpson (1981), and Coppin et al. (1991) presented data suggesting that λ has a constant value of 15, 6.5, and 6.5 respectively. Grassl (1976) and Schlüssel et al. (1990), in contrast, presented data suggesting that λ is wind speed dependent. They both presented the variation of λ with wind speed in tabular form, specifying different values of λ for different wind speeds. The λ values generally showed a near-linear increase with wind speed. Wu (1985, hereafter Wu) examined previous datasets and concluded that λ varies linearly with the wind speed up to 7 m s^{-1} but then is constant at greater wind speeds.

Hasse (1971) presented a model with the same functional form as that of Saunders. Hasse's (1971) development was different in that he attempted to obtain a solution for the temperature drop across a layer thicker than the skin layer. He also began with (1) but considered one layer where the thermal diffusivity was assigned the molecular value and a second layer where the thermal diffusivity was replaced with an eddy diffusivity. As with Saunders, Hasse took the thickness of the molecular layer to be inversely proportional to the wind speed, u, and found ΔT across that layer to be proportional to Q_N/u. Hasse speculated, however, that the functional behavior of the eddy diffusivity might add an additional term with a different wind speed dependence for the temperature drop beneath the molecular layer. To investigate this, Hasse modeled the eddy diffusivity and plotted the total temperature drop against Q_N/u. He found that even in the second layer, the temperature drop was still well represented by

$$\Delta T = C \frac{Q_N}{u}. \quad (5)$$

The value of his constant varied slightly with the depth of the bulk measurement but insignificantly with wind speed. Thus, Hasse's results were essentially the same as Saunders's with an invariant λ. For a bulk temperature measurement at a depth of 2.5 m, the value of the constant was found to be 1.48×10^{-2} m^3 K W^{-1} s^{-1}.

Equations (4) and (5) fail, however, as the wind speed approaches zero. In both cases the denominator approaches zero and the expression becomes undefined. As the wind speed approaches zero, there is a transition from a shear-driven to a free convection regime. Saunders addressed this fact and presented a second model for ΔT in the case of a dead calm. This relationship can be written

$$\Delta T \propto \left(\frac{\kappa\nu}{\alpha g}\right)^{1/4} \left(\frac{Q_N}{k}\right)^{3/4}, \quad (6)$$

where α is the coefficient of thermal expansion for water, g is acceleration due to gravity, and κ is the thermal diffusivity of water. Katsaros (1977) derived the same form from a classical analysis of thermal instability.

Fairall et al. (1995, hereafter Fairall) attempted to incorporate the free convection regime into a model of the form of (4) for use in the western Pacific warm pool. They accomplished this by smoothly blending expressions for the skin layer thickness in the shear-forced and free convection regimes. In the shear-forced regime, Fairall used the same form for the skin layer thickness as Saunders. The skin layer thickness in the free convection regime was derived from Rayleigh number scaling. The result was a new expression for λ incorporating both regimes. The expression is given by

$$\lambda = 6\left[1 + \left(\frac{16 Q_b g \alpha \rho_w c_p \nu^3}{u_*^4 k^2}\right)^{3/4}\right]^{-1/3}, \quad (7)$$

where Q_b is the virtual cooling given by

$$Q_b = Q_N + \left(\frac{S\beta c_p}{\alpha L_v}\right) Q_E, \quad (8)$$

c_p is the specific heat capacity of seawater at constant pressure, S is the salinity, β is the salinity expansion coefficient, L_v is the latent heat of vaporization of seawater, and Q_E is the latent heat flux. At wind speeds above approximately 3 m s^{-1}, λ approaches a constant value of 6. At lower wind speeds, λ varies with the wind speed.

Another group of models was developed from a different background based on the theory of surface renewal (Brutsaert 1975a,b; Liu and Businger 1975; Liu et al. 1979; Soloviev and Schlüssel 1994). The basic idea of the surface renewal theory is that the water in the skin layer is constantly renewed with bulk water from below. The bulk water reaches the surface and cools before it sinks again and is replaced with new water from below. The magnitude of ΔT is then related to the length of time that a parcel of water remains in contact with the interface.

Brutsaert (1975a) applied the theory of surface renewal to a study of evaporation rates but stated that his results would apply to heat transfer as well. He assumed that the renewal was accomplished by the smallest possible eddies. The length and timescales of these eddies are defined by the Kolmogorov microscales. He also assumed the heat transfer at the ocean surface oc-

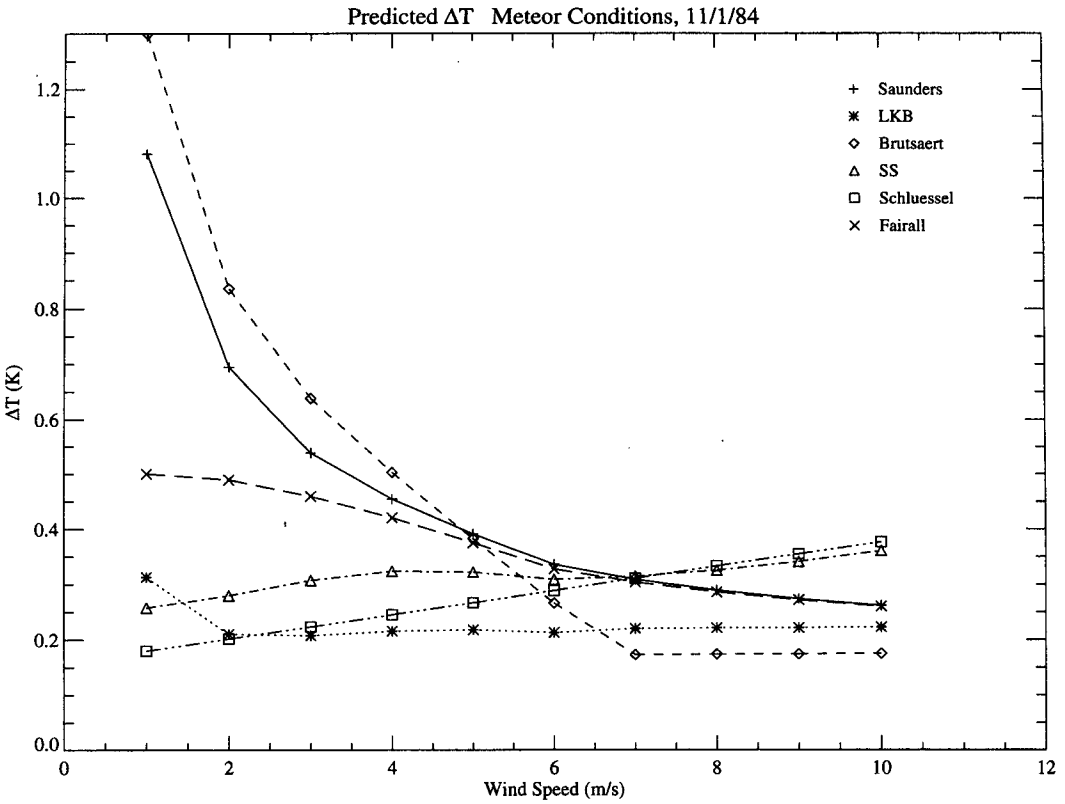

FIG. 5. Predicted response of ΔT to changes in wind speed in models by Saunders, LKB, Brutsaert, SS, Schlüssel, and Fairall. All meteorological and sea surface measurements were held constant except for wind speed. The predicted response thus includes changes in the net heat flux caused by wind speed changes. Note the tremendous differences in the predicted behavior of ΔT between the different models.

curred by molecular diffusion. By applying different expressions for diffusion and the skin layer thickness for smooth and rough surfaces, Brutsaert (1975a) then derived expressions for the evaporation rate from both surfaces. The equivalent expressions (hereafter referred to as Brutsaert) for heat transfer can be rearranged to give

$$\Delta T \propto \frac{Q_N}{\rho_w c_p u_*} \mathrm{Re}_r^{1/4} \mathrm{Pr}^{1/2} \tag{9}$$

for a rough surface and

$$\Delta T \propto \frac{Q_N}{\rho_w c_p u_*} \mathrm{Pr}^{2/3} \tag{10}$$

for a smooth surface, where $\mathrm{Re}_r = z_0 u_*/\nu$ is the roughness Reynolds number, z_0 is the momentum roughness length, and $\mathrm{Pr} = \nu/\kappa$ is the Prandtl number. Brutsaert (1975b) defined smooth surfaces to be where $\mathrm{Re}_r < 0.13$ and rough surfaces to be where $\mathrm{Re}_r > 2.0$. The proportionality constants for (9) and (10) as derived from available evaporation data were 7.3 and 13.6, respectively (Brutsaert 1975a). In this work, solutions in the transition region are found by interpolating linearly with Re_r between these limits.

Surface renewal theory was applied more specifically to the oceanic cool skin by Liu and Businger (1975), Liu et al. (1979), and Soloviev and Schlüssel (1994). Liu et al. (1979) and Soloviev and Schlüssel (1994) both followed a similar theoretical approach to Liu and Businger (1975) but assumed different expressions for the renewal timescale. By relating the average surface contact time, t_r, to the depth of a stagnant layer with an equivalent heat flux sustained by molecular diffusion, Liu and Businger (1975) found that

$$\Delta T \propto \frac{Q_N}{\rho_w c_p} \left(\frac{t_r}{\kappa}\right)^{1/2}. \tag{11}$$

Based on the work of Brutsaert (1975a), Liu et al. (1979, hereafter LKB) took the average surface contact time or time scale of surface renewal to be given by

$$t_r \propto (\nu z_0/u_*^3)^{1/2} \tag{12}$$

as derived from the Kolmogorov microscale. Their resulting model for ΔT is identical to (9) above. While LKB did not present a separate expression for smooth surfaces, they noted that the proportionality constant would depend on interfacial roughness characteristics

and that Re_r would approach a constant value for a smooth surface. These factors make their solution consistent with (10) also. Liu et al. (1979) found the proportionality constant for (9) to be 9.3 for conditions typical of the air–sea interface.

Soloviev and Schlüssel (1994, hereafter SS) adopted different renewal timescales for low, moderate, and high wind speed regimes. By doing this, SS successfully incorporated the free convection regime into their model. Their timescales for the convective, moderate, and high wind speed regimes were

$$t_r \propto (\nu \rho_w c_p / \alpha g Q_N)^{1/2}, \quad (13)$$

$$t_r \propto \nu / u_*^2, \quad (14)$$

and

$$t_r \propto u_* / g \quad (15)$$

respectively. Soloviev and Schlüssel (1994) defined the transition from free to forced convection in terms of a critical surface Richardson number. The surface Richardson number, defined by SS as $Rf_0 = -\alpha g Q_N \nu / \rho_w c_p u_*^4$, represents the ratio of buoyancy to shear forcing. Free convection was assumed to apply for $|Rf_0| > |Rf_{cr}| = 1.5 \times 10^{-4}$. Similarly the transition to high wind speed and long wave-breaking conditions was defined in terms of the Keulegan number, $Ke = u_*^3 / g\nu$. The high wind speed regime was defined as where $Ke > Ke_{cr} = 0.18$, which corresponded to a wind speed of 10 m s^{-1}. Soloviev and Schlüssel (1994) combined all of the regimes into a simplified expression given by

$$\Delta T / T_* = \Lambda_0 \, Pr^{1/2} (1 + Rf_0 / Rf_{cr})^{-1/4} \times (1 + Ke/Ke_{cr})^{1/2} \quad (16)$$

where $T_* = Q_N / \rho_w c_p u_*$ and Λ_0 was estimated as 13.3.

The final model for ΔT considered in this work was derived by Schlüssel et al. (1990) from the *Meteor* data. The model (referred to hereafter as Schlüssel) has the form

$$\Delta T = a_0 + a_1 u (T_s - T_a) + a_2 (q_s - q_a) + a_3 Q_{lw}, \quad (17)$$

where T_s is the ocean skin temperature, T_a is the air temperature, q_s is the saturation specific humidity, q_a is the specific humidity, and Q_{lw} is the net incoming longwave radiative flux. In contrast with the Saunders and surface-renewal-type models, this model is statistical in nature. The basic idea of ΔT being proportional to Q_N is the same, but each component of the net heat flux is considered separately. The coefficients derived by Schlüssel by regression against observations are $a_0 = -0.285$ K, $a_1 = 0.0115$ s m^{-1}, $a_2 = 37.255$ K, and $a_3 = -0.00212$ K m^2 W^{-1}. Though the model is statistical in nature, it was included for comparison since it was derived for the *Meteor* dataset being considered.

b. Equivalence of the models

The models are very similar in form despite the different derivations. The LKB and Brutsaert rough regime models are consistent with (4) if λ is assumed to be proportional to $Re_r^{1/4}$. This form for λ could explain the wind speed dependence in λ observed by Grassl (1976) and Schlüssel et al. (1990). The results of Wu, SS, and Fairall are all consistent in the sense that an equivalent λ is constant in some regimes and varies in others. Also, the results of SS for the moderate wind speed regime and Brutsaert's smooth regime model both agree with Saunders' model with a constant λ. The similarity between the SS and Saunders models occurs because the expression for the equivalent diffusion depth derived by SS has the same form as the skin-layer depth assumed by Saunders.

The similarity of the Saunders and surface-renewal-type models is not surprising considering the similarity of the physical mechanisms assumed in each approach. As long as there is no wave breaking or spray and the air–sea interface is intact, the heat transfer across the interface must occur by molecular processes. Thus, while a fluid element is in contact with the surface, the heat transfer will be by molecular diffusion. The only difference between the Saunders and surface renewal models is whether the fluid in contact with the atmosphere is assumed to remain there or be renewed from below.

TABLE 2. Statistics for the comparison of observed ΔT values with predictions of the published parameterizations. The bias is the mean difference between the observations and predictions, S.D. is the standard deviation of the differences, and r is the correlation coefficient between the observations and predictions.

	Saunders			Schlüssel			LKB			Brutsaert			SS			Fairall			Wu			Hasse		
Dataset	Bias (K)	S.D. (K)	r	Bias (K)	S.D. (K)	r	Bias (K)	S.D. (K)	r	Bias (K)	S.D. (K)	r	Bias (K)	S.D. (K)	r	Bias (K)	S.D. (K)	r	Bias (K)	S.D. (K)	r	Bias (K)	S.D. (K)	r
CEPEX	−0.01	0.04	.62	−0.15	0.06	.57	−0.07	0.04	.59	−0.04	0.08	.45	−0.01	0.04	.60	−0.01	0.04	.64	−0.01	0.04	.64	0.24	0.08	.66
Meteor	0.05	0.15	.32	−0.12	0.09	.78	−0.12	0.11	.73	0.02	0.22	.06	−0.03	0.10	.67	0.02	0.13	.38	0.01	0.10	.62	0.36	0.18	.44
Combined	0.02	0.12	.53	−0.13	0.08	.71	−0.10	0.09	.77	−0.01	0.17	.31	−0.02	0.08	.73	0.00	0.10	.58	0.00	0.08	.71	0.30	0.15	.61

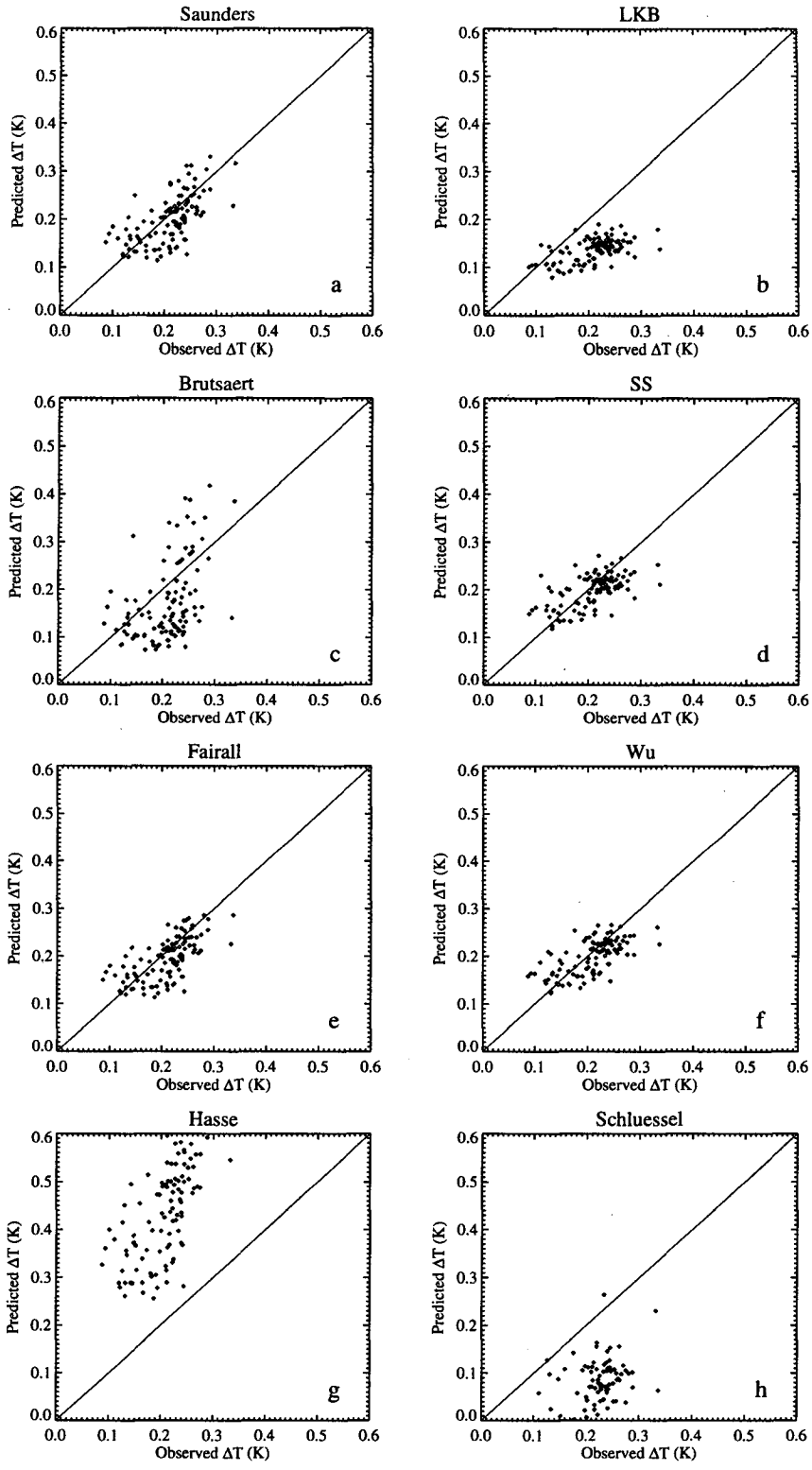

FIG. 6. Scatterplots demonstrating the relative ability of models by (a) Saunders, (b) LKB, (c) Brutsaert, (d) SS, (e) Fairall, (f) Wu, (g) Hasse, and (h) Schlüssel to predict ΔT measurements taken during CEPEX. Each diamond corresponds to an hour average of ΔT measurements and the solid line is the 1:1 line. The corresponding statistics are shown in Table 2. The majority of models predict the observed ΔT values during CEPEX reasonably well.

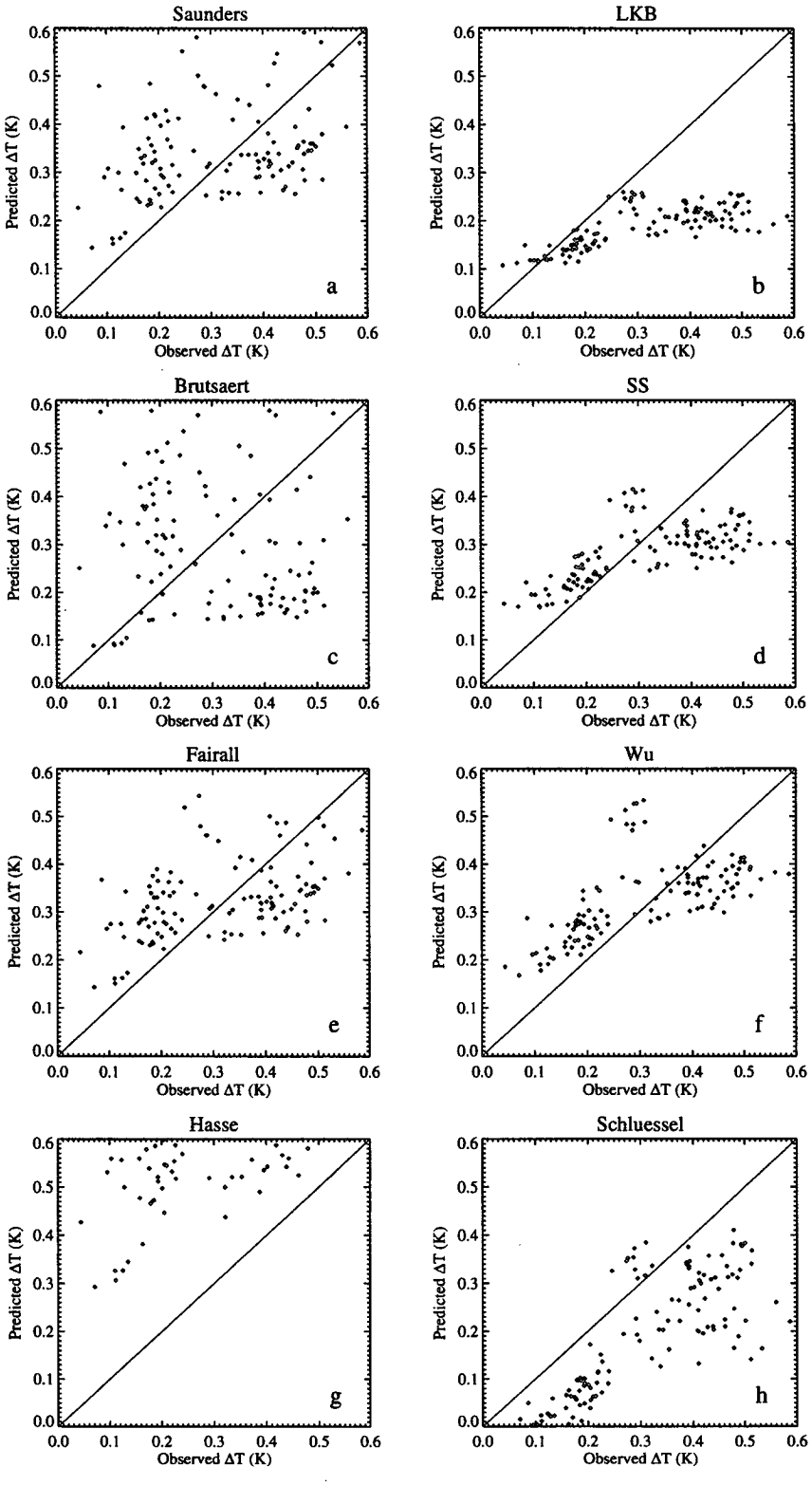

FIG. 7. Same as Fig. 6 but for measurements from the *Meteor*. In general, the models are not as successful in reproducing the observed ΔT values in the *Meteor* data.

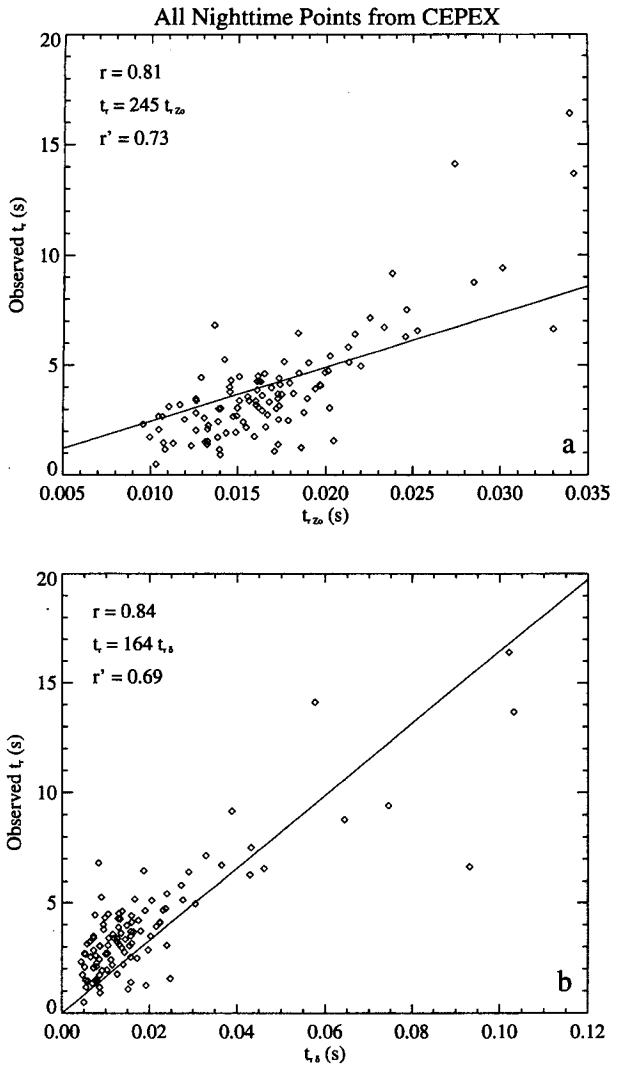

FIG. 8. Comparison between experimentally derived renewal timescale estimates with theoretical predictions from the (a) Z_0 (12) and (b) δ (14) timescales for nighttime measurements from CEPEX. Included in the figure are the correlation coefficient, equation of the line of best fit constrained to pass through the origin, and the square root of the coefficient of determination as defined in the text. The solid line is the plot of the line of best fit constrained to pass through the origin.

With the exception of the free convection and Schlüssel models, the model differences all correspond to the predicted dependence of ΔT on wind speed. The Hasse and Saunders models with constant λ predict that ΔT is proportional to either Q_N/u or Q_N/u_*. If λ depends on the wind speed, the relationship between ΔT and wind speed can be complicated. If λ varies linearly with the wind speed, however, the dependence on wind speed cancels out and ΔT is simply proportional to the net heat flux. If one substitutes Charnock's (1955) expression $z_0 = 0.11u_*^2/g$ into the definition of Re_r, the LKB and Brutsaert models predict that ΔT varies with $Q_N/u_*^{0.25}$. The predictions that ΔT is proportional to either Q_N/u_* or $Q_N/u_*^{0.25}$ are consistent with the observed two-part dependence of ΔT on wind speed described in the previous section. To determine the best model for ΔT, the precise dependence on wind speed must be determined.

The differences can be further traced back to one step in the derivation of the models from surface renewal theory. The bulk − skin temperature difference is related to the renewal timescale by (11). Since the oceanic mixed layer is a highly turbulent region, suppose that the renewal timescale must be comparable to the timescale of the smallest eddies present in the mixed layer. If so, the timescale should be proportional to the Kolmogorov microscale,

$$t_r \propto (\nu/\epsilon)^{1/2}, \tag{18}$$

where ϵ is the dissipation rate. The next step is to determine ϵ. Following Taylor (1935) as cited by Tennekes and Lumley (1972),

$$\epsilon \sim u^3/l, \tag{19}$$

where u is the characteristic velocity of the turbulent eddies and l is the integral length scale. If u_* and z_0 are taken as the characteristic velocity and length scale, respectively, t_r is given by (12) and hence ΔT is given by (9). If instead, $\epsilon \propto u_*^3/\delta$ and the skin layer thickness and renewal timescale are related by $\delta = (\kappa t_r)^{1/2}$ (Liu et al. 1979), solving for the renewal timescale gives

$$t_r \propto \frac{(\nu^2\kappa)^{1/3}}{u_*^2}. \tag{20}$$

This expression for t_r contains the same dependence on u_* as does (14). Inserting either (14) or (20) into (11) gives an expression of the form of (4), where the only difference is the value of λ and its dependence on the physical constants ν and κ.

Therefore, with the exception of Schlüssel's model, the basic models for ΔT in the shear-driven regime are consistent with one of two definitions of the dissipation rate. The dissipation rate then determines the wind speed dependence of ΔT. In the following section we compare the predicted timescales with experimentally derived values to determine which approach is most accurate. First, however, we investigate the effect the different formulations have on the predicted behavior of ΔT.

c. *Model-predicted ΔT behavior*

The response of a subset of models to changes in wind speed was compared under a set of conditions taken from the *Meteor* data. The wind speed was varied from 1 to 10 m s^{-1}, while all other measured quantities were held constant. The dependence of the heat flux on wind speed was included in the evaluation as the net

TABLE 3. Correlation coefficient, best fit slope, and coefficient of determination for comparisons between the observed and computed Z_0, δ, and convective renewal timescales.

	Z_{0t_r}						δ_{t_r}						Convective t_r		
	All nighttime points			$\lvert Rf_0\rvert < 1.5 \times 10^{-4}$			All nighttime points			$\lvert Rf_0\rvert < 1.5 \times 10^{-4}$			$\lvert Rf_0\rvert > 1.5 \times 10^{-4}$		
Dataset	r	Slope	r'	r	Slope	r'	r	Slope	r'	r	Slope	r'	r	Slope	r'
CEPEX	.81	245	.73	.56	209	.55	.84	164	.69	.57	221	.25	.33	3.13	.33
Meteor	.49	253	.48	.18	243	.10	.52	102	.19	.15	204	undef.	.03	2.29	undef.

heat flux varied with the changes in wind speed. In this manner, the net effect of a wind speed change on ΔT is observed. A subset of the models was used for clarity since many of the models are similar. The scheme labeled Saunders used a constant λ value of 6.0.

The results of the comparison are shown in Fig. 5. The differences in the predicted wind speed dependence lead to a dramatic difference in the predicted behavior of ΔT. The Schlüssel and SS models predict that the largest ΔT will occur at the largest wind speed, while all the other models predict that the largest ΔT occurs at the smallest wind speed. The Saunders and Brutsaert models predict the strongest increase in ΔT as the wind speed decreases. The LKB model also predicts a sharp increase in ΔT as the wind speed decreases, but only below approximately 2 m s^{-1}. The Saunders and Fairall models are identical at larger wind speed, but the Fairall model predicts a downturn in ΔT at low wind speeds in the transition into the free convection regime. The SS model also predicts a downturn in ΔT as it transitions into the free convection regime, but the transition occurs at a larger wind speed leading to the predicted decrease in ΔT at the lowest wind speeds. Only the Schlüssel and SS models predict an increase in ΔT with wind speed at a wind speed of 10 m s^{-1}. The Schlüssel model predicts a linear increase in ΔT with wind speed throughout the range of conditions. The increase in ΔT with wind speed in the SS model at high wind speeds occurs as a result of the transition from the moderate to high wind speed regime. In contrast, the Brutsaert and LKB models predict almost no change in ΔT with wind speed at high wind speeds, and the Saunders and Fairall models predict a slight decrease in ΔT with wind speed. Similar computations using the CEPEX data showed the same tendencies.

4. Comparison of theories with in situ data

The wide variation between the predicted ΔT values underscores the need to determine which, if any, of the models most accurately reproduces ΔT. To quantitatively determine which approach is more accurate, it is necessary to compare individual predicted values with observations. Each model described above was evaluated using the nighttime hourly averaged measurements from the *Meteor* and CEPEX. The mean difference, standard deviation, and correlation coefficient between the observed and predicted ΔT values are listed in Table 2.

The success of the models as measured by the statistics varies between the datasets. For the CEPEX data, the means and standard deviations of the differences between the observed and predicted ΔTs for each model are generally small. In several cases, the mean difference is less than 0.02 K and the standard deviation is near 0.04 K. These figures indicate that the models predict ΔT well at least in an average sense. Based on these numbers, an expected error in a ΔT estimate would be on the order of 0.05 K. The correlation coefficients, however, are not very high. This suggests there is still significant scatter and the models may not be predicting all the variability in ΔT such as caused by variations in the wind speed. No single model does significantly better than the others for the CEPEX data, but the models with t_r given by (14) (Saunders, SS, Fairall) do have lower biases than the models with t_r given by (12) (LKB; Brutsaert). The standard deviations and correlation coefficients are very similar for all the models. The Schlüssel and Hasse models have the only large biases. The large bias in the Schlüssel model could be the result of the errors in the *Meteor* 2-m bulk temperature from which the model was derived. The bias in the Hasse model could indicate a problem with the proportionality constant assumed by Hasse.

The accuracy of the models varies more for the *Meteor* data. For some models, the correlation coefficients are higher than for the CEPEX data, but for others the standard deviation is larger. From the statistics alone, the Wu and SS models appear to better predict ΔT. Both of these models incorporate different wind speed dependencies for different regimes. The expected errors in the predicted ΔT values for the *Meteor* data are on the order of 0.1 K.

The statistics were also computed for the two datasets combined. The overall biases are smallest for the Fairall and Wu models. The SS model has a slightly larger bias but also a slightly larger correlation coefficient. The LKB and Schlüssel models have the largest correlation coefficients but they both have larger biases. Statistically, the SS and Wu models

perform the best overall as they did for the *Meteor* data.

The greatest concern about the applicability of the models is the low correlations between the observed and predicted ΔT values. To further evaluate the performance of the models, the observed ΔT values were plotted against the ΔT values predicted with each model. The plots from CEPEX are shown in Fig. 6 and the plots from the *Meteor* are shown in Fig. 7. The scatterplots computed from the CEPEX data again illustrate that the majority of models estimate ΔT well. The scatter in the Saunders, SS, Fairall, Wu, and Hasse models appears to be consistent with only random errors. The errors in the remaining models, however, suggest some systematic errors in the calculations. The majority of scatter in the Brutsaert model is from points in the transition regime where solutions were interpolated linearly between the smooth and rough regimes. Results confined to the smooth and rough regimes are as good as the other parameterizations. The scatterplots from the *Meteor* data indicate that the models are not as successful in predicting the ΔT values observed in the *Meteor* data. The Wu and SS models predict ΔT reasonably well, but the scatter no longer appears only random in nature. The predictions of the Saunders and Fairall models are poorly correlated with the observations. The predictions with the LKB model are the most highly correlated to the observed ΔT values but systematically underestimate the observations at all but the smallest ΔT values.

From the statistics and plots above it is difficult to conclude which model is most accurate. Because of variations in the proportionality constants, we evaluated the basic model forms to determine which renewal timescale and corresponding wind speed dependence most accurately reflects the observed behavior. Experimentally derived values for the renewal timescale were plotted against the theoretically predicted values presented in (12)–(15). Although the renewal timescale could not be directly measured, it was estimated from the ΔT measurements using (11). Differences between the derived and predicted timescales could then be caused by errors either in the theoretical predictions or the assumptions used to derive (11). The data were

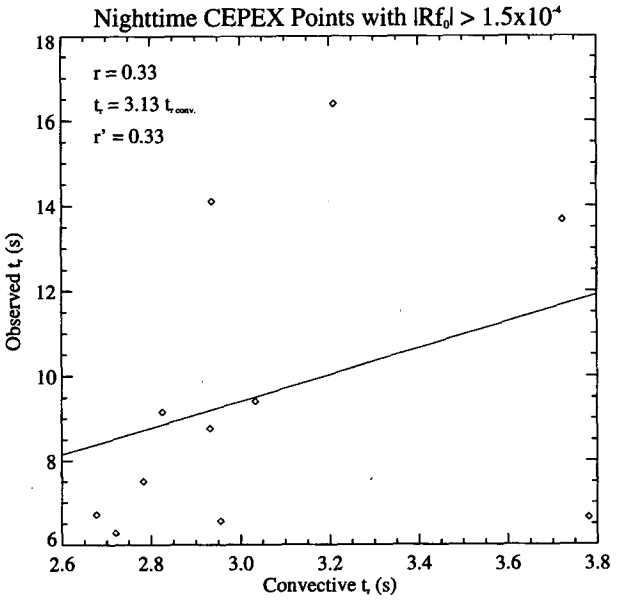

FIG. 9. Comparison between experimentally derived renewal timescale estimates with theoretical predictions using the convective renewal timescale (13) from the CEPEX data. Only measurements corresponding to $|Rf_0| > 1.5 \times 10^{-4}$ are included to isolate conditions in the free convection regime. The correlation coefficient, line of best fit constrained to pass through the origin, and square root of the coefficient of determination are again included. The correlation coefficient and coefficient of determination are very low, but there are few points in the free convection regime.

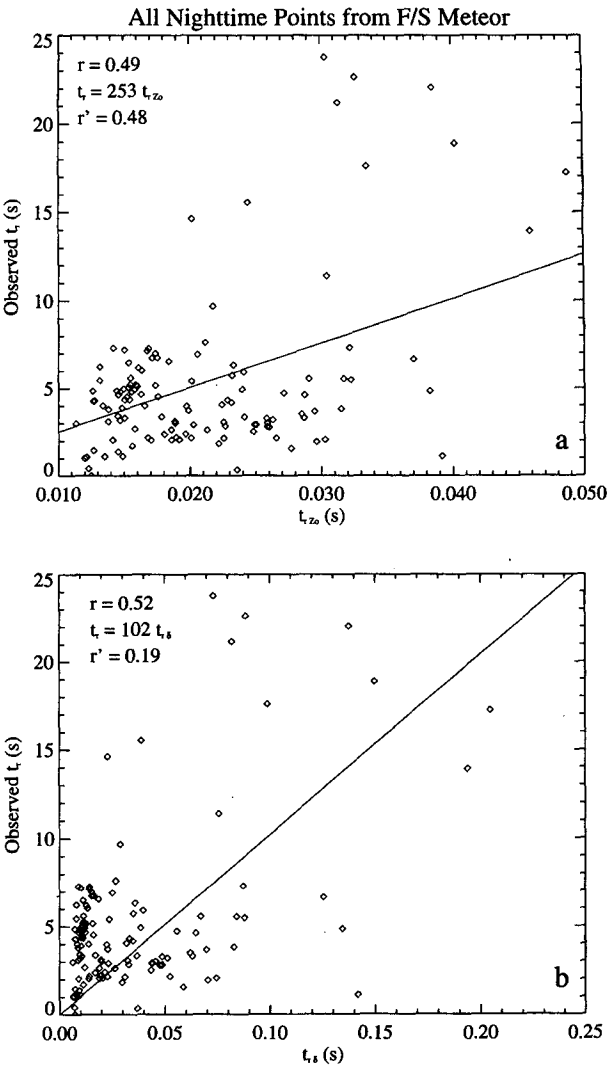

FIG. 10. Same as Fig. 8 but for measurements from the *Meteor*.

TABLE 4. Values of the proportionality constants and critical surface Richardson number for each dataset.

Dataset	C_{shear}	C_{conv}	Rf_{cr}
CEPEX	209	3.13	-2.25×10^{-4}
Meteor	244	2.29	-8.87×10^{-5}

also sorted by surface Richardson number to enable the convective renewal timescale to be tested.

Two quantities were calculated to quantify the ability of each theoretical timescale to reproduce the observed

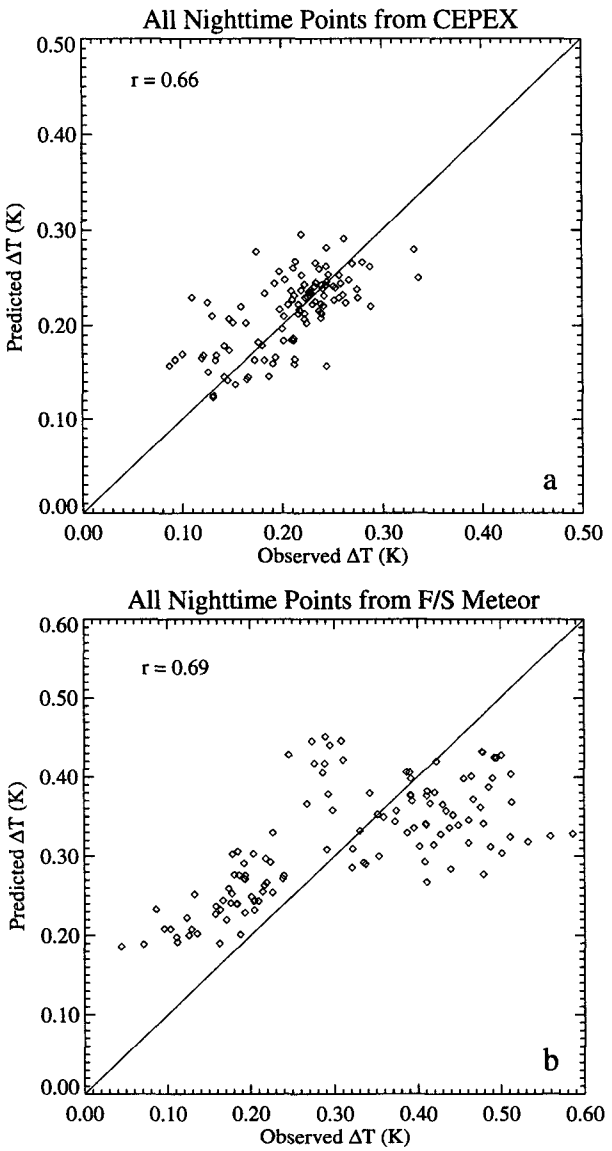

FIG. 11. Comparison of ΔT values predicted using (23) with nighttime measurements from the (a) CEPEX and (b) *Meteor* data. The correlation coefficient and 1:1 line are also shown in the figure. Additional statistics for the comparisons are included in Table 5. In both cases, the new model does at least as well as all of the previous models in predicting ΔT.

t_r values. The first was the usual correlation coefficient, r, between the experimental and predicted timescales. The second was the coefficient of determination, r'^2, based on a linear least squares fit to the data constrained to pass through the origin. The normal correlation coefficient is a measure of the degree of linearity between the experimental and predicted timescales when the intercept is not constrained in any way. For the expressions in (12)–(15) to hold, however, the experimental timescale should be related to the theoretical form by only a constant multiple and the intercept must be zero. An additional quantity was required to quantify the goodness of fit of a line constrained to pass through the origin. The coefficient of determination was calculated for this constraint. The coefficient of determination, defined as

$$r'^2 = 1 - \frac{\Sigma\,(t_{r_{observed}} - t_{r_{predicted}})^2}{\Sigma\,(t_{r_{observed}} - \overline{t_{r_{observed}}})^2}, \qquad (21)$$

where the overbar denotes an average value, is a measure of the percent of variance explained by the fit. The values were presented as r' rather than r'^2 to make them comparable to the correlation coefficient.

The renewal timescales computed using (12) (called the Z_0 timescale to emphasize the use of z_0 as the length scale) are plotted against the experimentally derived timescales for the CEPEX data in Fig. 8a. The results when the timescales were computed using (14) (the δ timescale for the use of δ as the length scale) are similarly shown in Fig. 8b. The correlation coefficient, least squares fit slope, and coefficient of determination are included in the figures and Table 3. In the table, values are shown separately for all points and only those where $|Rf_0| < 1.5 \times 10^{-4}$ (shear-driven). An undefined value of r' indicates the coefficient of determination, r'^2, was negative.

Both Z_0 and δ predicted timescales are well correlated with the derived renewal timescale. The agreement provides support for the assumption that there is a renewal timescale associated with the ocean skin and hence surface renewal theory. The correlation coefficients are very similar for the Z_0 and δ timescales, but the coefficient of determination is greater for the Z_0 timescale especially when the data are limited to $|Rf_0| < 1.5 \times 10^{-4}$. The Z_0 timescale thus provides a better fit to the data when the linear relationship is forced to pass through the origin. The linear fit explains a larger portion of the variance when all the points are consid-

TABLE 5. Statistics for the comparison of ΔT computed with (23) to the observed values. The bias and standard deviation (S.D.) are computed for the difference $\Delta T_{observed} - \Delta T_{predicted}$.

Dataset	Bias (K)	S.D. (K)	r
CEPEX	0.006	0.038	.66
Meteor	0.003	0.098	.69

ered. This is due to the larger range of timescales that occurs when the lower wind speed conditions are included. Despite the fact that r and r' are lower for the points with $|\mathrm{Rf}_0| < 1.5 \times 10^{-4}$, the scatter appears to be consistent with random measurement errors. There is little difference between r and r' for the Z_0 timescale at low surface Richardson numbers implying that the intercept of the unconstrained line of best fit is very close to the origin. This provides additional support for the Z_0 timescale.

The renewal timescales computed using the convective timescale (13) are plotted against the experimental values for the CEPEX points where $|\mathrm{Rf}_0| > 1.5 \times 10^{-4}$ in Fig. 9. The correlation is significantly lower than for the other timescales, but there are too few points to draw any conclusions about the accuracy of the convective timescale. The convective timescale is well supported by many theoretical studies on convection. The agreement between the points in Fig. 9 and the shear-driven timescales above could indicate that $|\mathrm{Rf}_{cr}|$ is set too low and these points still fall within the shear-driven regime.

Plots comparing the experimental timescales from the *Meteor* data with the Z_0 and δ renewal timescales are shown in Fig. 10 and the statistics are included in Table 3 as for the CEPEX data. The majority of data points support a relationship between the experimental and calculated timescales, but a few points are widely scattered and decrease r and r'. Only two of these points correspond to a $|\mathrm{Rf}_0| < 1.5 \times 10^{-4}$. These points occur sequentially on the last day of data and have values of Rf_0 just within the limiting value. If those two points are removed from the set of points with $|\mathrm{Rf}_0| < 1.5 \times 10^{-4}$, the correlation coefficients for the Z_0 and δ timescales rise to 0.51 and 0.56, respectively, r' for the Z_0 timescale increases to 0.51, and r' for the δ timescale becomes defined with a value of 0.18. The proportionality constant for the Z_0 timescale is changed to 244. This value differs from the CEPEX value by only 20%. The values of r' and the proportionality constant indicate that the *Meteor* data is described reasonably well by the Z_0 timescale. No significant correlation was observed between the experimental and convective timescales for the *Meteor* data.

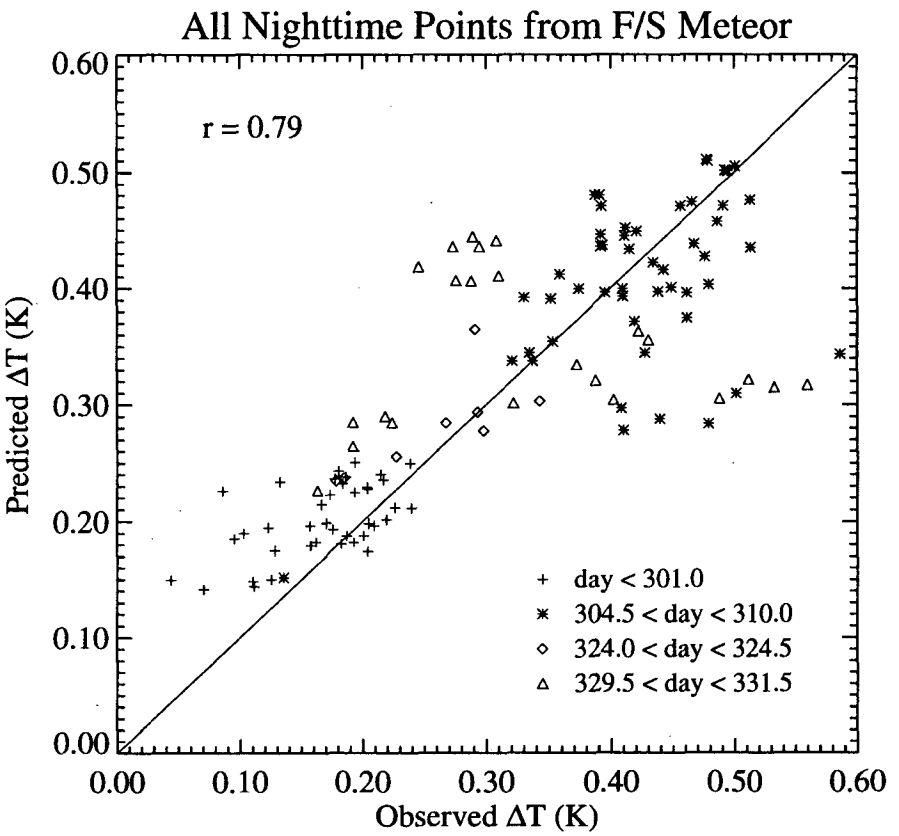

FIG. 12. Comparison between observed ΔT values from the *Meteor* with predictions using (23) when separate proportionality constants were derived for individual cruise segments. Note the improvement over Fig. 11b, where the proportionality constants were derived for the entire dataset. The new ΔT model performs well for all but the last cruise segment as indicated by the triangles in the figure.

Based on the results from each dataset, the data appear consistent with surface renewal theory and an associated renewal timescale for the water at the skin of the ocean. The renewal timescale defined by (12; Z_0) was slightly more successful than the scale defined by (14; δ) in describing the behavior of ΔT in the shear-driven regime. The differences between the two timescales were not pronounced as both were subject to large amounts of scatter. The scatter makes it difficult to significantly conclude which timescale is more accurate. Nevertheless, both datasets were fit better when the Z_0 timescale was used. The Z_0 timescale was shown here to be derived from the Kolmogorov microscale with the dissipation rate defined in terms of the friction velocity and the roughness length. As described earlier, this solution is equivalent to defining a λ value for (4) that varies with wind speed through $\mathrm{Re}_r^{1/4}$. Using Charnock's equation (1955), this corresponds to a dependence of ΔT on wind speed of $\Delta T \propto u_*^{-0.25}$.

New ΔT model

Based on these findings, the optimum nighttime model for ΔT should be given by (11) with the renewal timescale defined by (12) in the shear-driven regime. To apply the model under all conditions up to the onset of wave breaking, the renewal timescale should incorporate both the shear-driven and free convection timescales. While our data did not support a convective timescale given by (13), the CEPEX and *Meteor* data had few points in the convective regime and the expression is supported by theoretical and other experimental results.

The transition from the shear-driven to free convection regime is smooth implying there should be a smooth transition between the timescales. Following SS, the transition should be governed by Rf_0. The convective timescale strictly applies only when the wind speed is zero and, thus, when Rf_0 becomes infinite. The renewal timescale should take on the convective value only in this limit. The data suggested that the shear-driven timescale should dominate at all but the highest values of Rf_0. A relationship for t_r incorporating these characteristics is

$$t_r = t_{r_{\mathrm{shear}}} + (t_{r_{\mathrm{conv}}} - t_{r_{\mathrm{shear}}})e^{-C/\mathrm{Rf}_0}, \qquad (22)$$

where C is a constant that controls the Rf_0 value at which the influence of the convective scale become significant. For this model, C was set equal to $\mathrm{Rf}_{\mathrm{cr}}$. The renewal timescale is then about 37% controlled by the convective value at $\mathrm{Rf}_0 = \mathrm{Rf}_{\mathrm{cr}}$. The influence of the convective value rapidly becomes greater as $|\mathrm{Rf}_0|$ becomes greater than $|\mathrm{Rf}_{\mathrm{cr}}|$.

The appropriate value of $\mathrm{Rf}_{\mathrm{cr}}$ was investigated with both datasets. Soloviev and Schlüssel (1994) stated that $\mathrm{Rf}_{\mathrm{cr}} = -(C_{\mathrm{conv}}/C_{\mathrm{shear}})^2$, where C_{conv} and C_{shear} are the proportionality constants for the convective and shear-driven timescales. Values of $\mathrm{Rf}_{\mathrm{cr}}$ were computed for each dataset using the best fit slopes for the Z_0 and convective timescales presented above. The proportionality constants and resulting $\mathrm{Rf}_{\mathrm{cr}}$ values are shown in Table 4. We used the average of the two $\mathrm{Rf}_{\mathrm{cr}}$ values, -1.6×10^{-4} in (22). This value is in good agreement with the value $\mathrm{Rf}_{\mathrm{cr}} = -1.5 \times 10^{-4}$ used by SS.

The new ΔT model derived from this work uses (11) and (22) with $t_{r_{\mathrm{shear}}}$ and $t_{r_{\mathrm{conv}}}$ defined by (12) and (13), respectively. Combining these, the model can be written

$$\Delta T = \frac{Q_N}{\rho_w c_p \kappa^{1/2}} \left\{ C_{\mathrm{shear}} \left(\frac{\nu z_0}{u_*^3} \right)^{1/2} + \left[C_{\mathrm{conv}} \left(\frac{\nu \rho_w c_p}{\alpha g Q_N} \right)^{1/2} - C_{\mathrm{shear}} \left(\frac{\nu z_0}{u_*^3} \right)^{1/2} \right] e^{-(\mathrm{Rf}_{\mathrm{cr}}/\mathrm{Rf}_0)} \right\}^{1/2}. \qquad (23)$$

The proportionality constants were applied individually for each dataset because of potential calibration differences between the datasets. The values used are those shown in Table 4. This model was applied to each dataset to compare its effectiveness to that of the previously published models.

The ΔT estimates calculated with (23) are plotted against the observed ΔT values for the CEPEX and *Meteor* datasets in Figs. 11a and 11b, respectively. The mean differences, standard deviations of the differences, and correlation coefficients are shown in Table 5 as for the previous models. The new model performs as well or better than the previous models for both datasets. It is true that the model used different proportionality constants for the two datasets, but the constants did not vary that much. In both cases the mean difference is less than 0.01 K and the standard deviation is less than 0.1 K. The average errors are, therefore, 0.1 K or less for each dataset. This error level is at the error level of the individual ΔT measurements.

The scatterplot for the *Meteor* data illustrates a slight problem where the model tends to overestimate ΔT at low values and underestimate ΔT at high values. The same tendency could be observed in some of the previous models. The *Meteor* points were sorted by Re_r, Rf_0, and date to determine if the data clusters apparent in Fig. 11b corresponded to specific conditions. This would indicate if the model was not performing well in a certain regime. The points corresponding to specific ranges of Re_r and Rf_0 were distributed throughout the plot and did not group into clusters. The clusters did, however, correspond to specific measurement dates. When separate coefficients were derived for each date range, the predicted ΔT values shown in Fig. 12 were obtained. The agreement between the observed and predicted ΔT values in Fig. 12 is better than when measurements from the entire cruise were grouped together. The correlation coefficient is increased to 0.79 and the standard deviation is reduced to 0.082 K. The bias increased slightly to 0.009 K. These results suggest that the errors in the ΔT predictions are largely caused

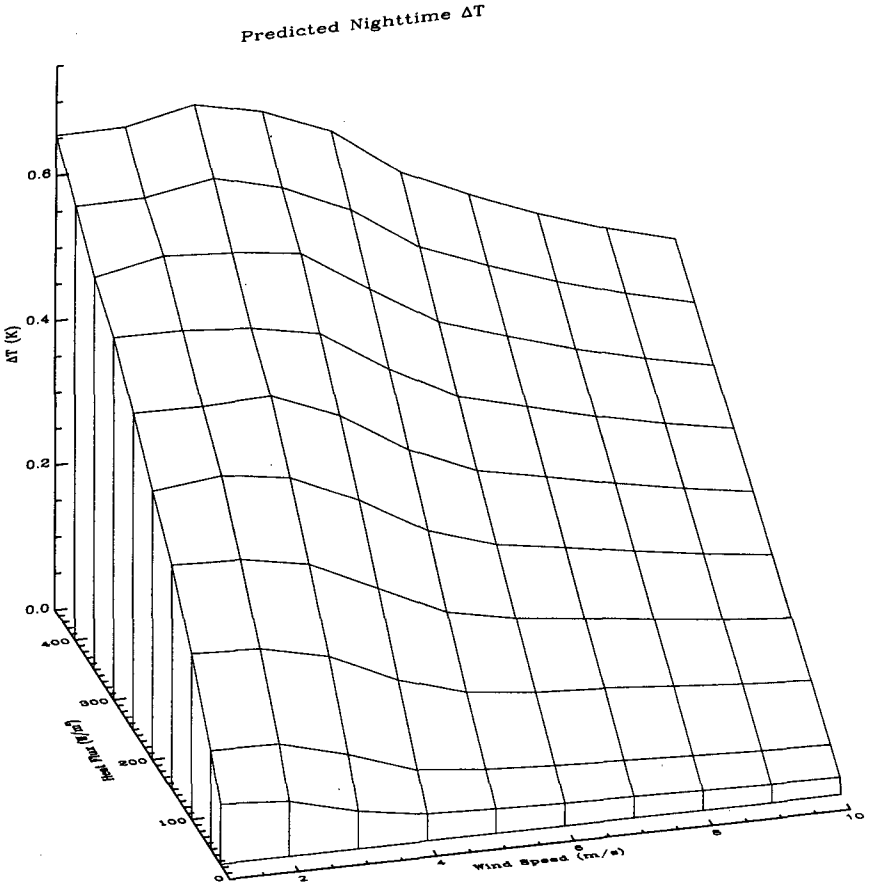

FIG. 13. Response of ΔT to changes in net heat flux and wind speed as predicted by (23). The predicted behavior generally agrees with the behavior observed in the *Meteor* and CEPEX datasets in Fig. 3.

by instrumental differences during different portions of the cruise rather than the failure of (23) to properly reproduce certain regimes. Other possible reasons for errors in the predicted ΔT values are the effects of small-scale wave breaking (Wu 1995) and the lack of exact coincidence between the heat flux and ΔT measurements.

The wind speed dependence predicted by the new model is summarized by plotting ΔT as a simultaneous function of wind speed and net heat flux as for the observed datasets. The resulting plot is shown in Fig. 13. The predicted behavior has the same tendencies as were observed in the CEPEX and *Meteor* data in Figs. 3a and 3b. The bulk − skin temperature difference increases with heat flux at constant wind speeds and increases as the wind speed decreases down to a wind speed between 2 and 3 m s^{-1} when the heat flux is held constant. Below wind speeds of 2 m s^{-1}, the model predicts a downturn in ΔT as the free convection regime is approached. This is in contrast to the extremely high values predicted at low wind speeds by the Saunders, Hasse, and Brutsaert models. There were too few points in this regime in the in situ datasets to verify the behavior in this regime. The model predicts that the increase in ΔT with heat flux at constant wind speed is linear. The observations are not inconsistent with this behavior, but the random errors in the observations are too large to conclusively verify this behavior.

From the behavior illustrated in Fig. 13, it is possible to see how changes in wind speed can have a different effect on ΔT depending on the current conditions. A contour plot corresponding to the surface in Fig. 13 was generated and is shown in Fig. 14. The conditions from the *Meteor* data used to generate Fig. 5 were taken and the relative humidity was modified to simulate very moist and dry conditions. The wind speed was varied from 1 to 10 m s^{-1} while holding the other conditions constant at relative humidity values of 50% and 85%. The relationship between the net heat flux and wind speed for the dry and wet conditions are indicated by the dotted and dashed lines, respectively. The effect of the wind speed change on ΔT is very different under the two conditions. Under the moist conditions and corresponding low latent heat flux, the effects of heat flux

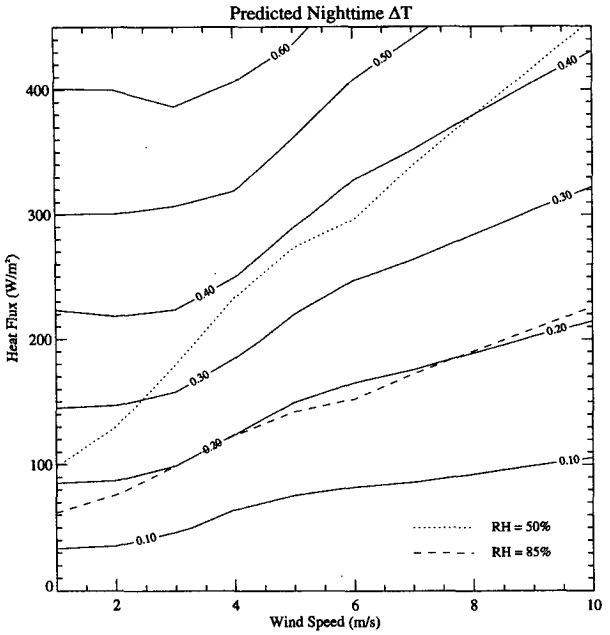

FIG. 14. This figure illustrates different possible responses of ΔT to a change in wind speed. The contours represent the ΔT values predicted by (23) for the corresponding net heat flux and wind speed values. The dotted line represents the change in heat flux corresponding to a change in wind speed from 1 to 10 m s^{-1} when the relative humidity is arbitrarily held constant at 50%. All other conditions were taken from data collected on 1 November 1984 aboard the *Meteor*. The dashed line is for a constant relative humidity of 85%. While the change in wind speed leads to almost no change in ΔT under the moist conditions, the same change in wind speed corresponds to nearly a 0.2 K increase in ΔT under dry conditions.

and turbulent mixing nearly cancel and ΔT changes by only about 0.05 K. Under dry conditions, however, the effect of wind speed on the net heat flux dominates. The net heat flux increases by over 300 W m^{-2}, causing ΔT to increase by nearly 0.2 K. Through accurate models, the effect of wind speed on ΔT can be predicted under arbitrary conditions.

5. Conclusions

Wind speed affects the magnitude of ΔT through both turbulent mixing and the net heat flux. A rise in wind speed enhances the turbulent mixing in the ocean and typically increases the heat flux. The increased mixing causes ΔT to decrease while the increased heat flux causes ΔT to increase. In situ observations of ΔT indeed show ΔT to increase with the heat flux when the wind speed is held constant and decrease with increasing wind speed when the heat flux is held constant. As wind speed changes affect the net heat flux, the effect on ΔT is dependent on the current conditions and the relative effect of the wind speed change on the net heat flux. An accurate model of ΔT is required to predict the net effect on ΔT due to simultaneous changes in wind speed and the net heat flux.

All the previously published models for the shear-driven regime were shown to be consistent with one derivation from surface renewal theory. The difference in form of the models results from a different definition of the dissipation rate. The net effect of the difference is to change the predicted dependence of ΔT on wind speed. The models in the free convection regime are also consistent with surface renewal theory. Present in situ data supports the surface renewal theory and best fits a dissipation rate derived using the roughness length scale as proposed originally by Brutsaert (1975a) and Liu et al. (1979). The resulting model for ΔT predicts that ΔT is proportional to $Q_N \mathrm{Re}_r^{0.25}/u_*$, rather than simply Q_N/u_* as originally proposed by Saunders.

A new model was presented based on these findings. The model contained both free convection and shear-driven regimes with the transition governed by the surface Richardson number. The model was able to reproduce both aspects of the dependence of ΔT on wind speed observed in the data and reproduced observations of ΔT in both the midlatitude Atlantic and tropical Pacific to an accuracy of better than 0.1 K.

Acknowledgments. The authors gratefully acknowledge the support of the National Aeronautics and Space Administration and program managers Bill Patzert and Mike Van Woert under Grant NAGW1110. The participation of Peter Schlüssel was supported in part by the German Research Agency (DFG). We thank the crews of the R/V *John V. Vickers* and F/S *Meteor* for their help in the collection of the data used in this paper. Finally, we also thank the anonymous reviewers for their comments, which led to a much improved version of this paper.

REFERENCES

Brutsaert, W., 1975a: A theory for local evaporation (or heat transfer) from rough and smooth surfaces at ground level. *Water Resour. Res.*, **11,** 543–550.

——, 1975b: The roughness length for water vapor, sensible heat, and other scalars. *J. Atmos. Sci.*, **32,** 2028–2031.

Charnock, H., 1955: Wind stress on a water surface. *Quart. J. Roy. Meteor. Soc.*, **81,** 639–640.

Clayson, C. A., C. W. Fairall, and J. A. Curry, 1996: Determination of the net oceanic surface fluxes of heat, freshwater, and momentum. *J. Geophys. Res.*, in press.

Coppin, P. A., E. F. Bradley, I. J. Barton, and J. S. Godfrey, 1991: Simultaneous observations of sea surface temperature in the western equatorial Pacific by bulk, radiative and satellite methods. *J. Geophys. Res.*, **96,** 3401–3409.

Ewing, G., and E. D. McAlister, 1960: On the thermal boundary layer of the ocean. *Science,* **131,** 1374–1376.

Fairall, C. W., E. F. Bradley, J. S. Godfrey, G. A. Wick, J. B. Edson, and G. S. Young, 1996: Cool skin and warm layer effects on sea surface temperature. *J. Geophys. Res.*, **101,** 1295–1308.

Grassl, H., 1976: The dependence of the measured cool skin of the ocean on wind stress and total heat flux. *Bound.-Layer Meteor.*, **10,** 465–474.

Hasse, L., 1971: The sea surface temperature deviation and the heat flow at the sea-air interface. *Bound.-Layer Meteor.*, **1,** 368–379.

Katsaros, K. B., 1977: The sea surface temperature deviation at very low wind speeds; Is there a limit? *Tellus,* **29,** 229–239.

——, 1980: The aqueous thermal boundary layer. *Bound.-Layer Meteor.*, **18,** 107–127.

Liu, W. T., and J. A. Businger, 1975: Temperature profile in the molecular sublayer near the interface of a fluid in turbulent motion. *Geophys. Res. Lett.*, **2,** 403–404.

——, K. B. Katsaros, and J. A. Businger, 1979: Bulk parameterization of air–sea exchanges of heat and water vapor including the molecular constraints at the interface. *J. Atmos. Sci.*, **36,** 1722–1735.

McAlister, E. D., and W. McLeish, 1969: Heat transfer in the top millimeter of the ocean. *J. Geophys. Res.*, **74,** 3408–3414.

Paulson, C. A., and T. W. Parker, 1972: Cooling of a water surface by evaporation, radiation, and heat transfer. *J. Geophys. Res.*, **77,** 491–495.

——, and J. J. Simpson, 1981: The temperature difference across the cool skin of the ocean. *J. Geophys. Res.*, **86,** 11 044–11 054.

Robinson, I. A., N. C. Wells, and H. Charnock, 1984: The sea surface thermal boundary layer and its relevance to the measurement of sea surface temperature by airborne and spaceborne radiometers. *Int. J. Remote Sens.*, **5,** 19–45.

Saunders, P. M., 1967: The temperature at the ocean–air interface. *J. Atmos. Sci.*, **24,** 269–273.

Schlüssel, P., W. J. Emery, H. Grassl, and T. Mammen, 1990: On the bulk – skin temperature difference and its impact on satellite remote sensing of sea surface temperature. *J. Geophys. Res.*, **95,** 13 341–13 356.

Soloviev, A. V., and P. Schlüssel, 1994: Parameterization of the cool skin of the ocean and of the air–ocean gas transfer on the basis of modeling surface renewal. *J. Phys. Oceanogr.*, **24,** 1339–1346.

Taylor, G. I., 1935: Statistical theory of turbulence, *Proc. Roy. Soc. London Ser. A,* **151,** 421–444.

Tennekes, H., and J. L. Lumley, 1972: *A First Course in Turbulence.* MIT Press, 300 pp.

Wu, J., 1985: On the cool skin of the ocean. *Bound.-Layer Meteor.*, **31,** 203–207.

——, 1995: Small-scale wave breaking: A widespread sea surface phenomenon and its consequence for air–sea exchanges. *J. Phys. Oceanogr.*, **25,** 407–412.